16th World Conference on Earthquake Engineering, 16WCEE 2017
Santiago Chile, January 9th to 13th 2017
Paper N° 4859
Registration Code: S-XXXXXXXX

THE ENERGY DISSIPATION AND MECHANICAL CHARACTERISTICS OF A NEW 3D SEISMIC ISOLATION SYSTEM

M. Imam[1], W.G. Liu[2], W.F. He[3], Q.R. Yang[4]

[1] Ph.D., Candidate, Shanghai University, China, mostafaa_@msn.com
[2] Prof., Shanghai University, China, liuwg@aliyun.com
[3] Associate Prof., Shanghai University, China, 35702305@qq.com
[4] Associate Prof., Shanghai University, China, yangqr@shu.edu.cn

Abstract

Vertical earthquake components are usually insignificant during seismic analysis and design, whereas a safe design for the horizontal seismic responses is assumed to accommodate the forces generated due to vertical seismic excitations. This assumed safety limit is in accordance with the acceptance criteria specified by some of the major design standards that deal with vertical seismic accelerations. While the aforementioned approach may be true for some types of structures or areas of a certain level of seismicity, there are multiple considerations that could invalidate this approach. Such considerations can include types of structures that contain dangerous chemical substances or those which are of critical national importance such as nuclear power plants. Furthermore, time history records for multiple earthquakes such as TAFT, KOBE and HACHINOHE combined with horizontal seismic isolation for certain types of heavy structures have shown a significant response in the vertical direction that could not be accommodated by traditional design methods indicated within most seismic design standards.

Previous investigations such as that carried out for 3D seismic isolation of Fast Breeder Reactors in Japan have introduced 3D seismic isolation within the engineering community, where this study has shown the significance of the vertical earthquake components on these types of structures as well as offering particular concepts and strategies that can be used to mitigate such responses, these concepts are briefly introduced. As there is an obvious need for more research in this area, where there are only a few concepts covering vertical seismic isolation worldwide, this paper introduces a research project carried out in order to verify a new concept for a 3D seismic isolation device called 3D Rotational Seismic Isolator abbreviated as 3DRSI. This device was developed and investigated as a part of an ongoing research to obtain economical and flexible solutions for mitigation of both horizontal and vertical seismic excitations.

The target of this research was achieved by the development of the concept, defining components, researching the variable parameters, testing of three specimens to verify the mechanical and energy dissipation characteristics.

Keywords: 3D Seismic isolation; Vertical seismic isolation; Vertical energy dissipation; Lead rubber bearings

1. Introduction

Since two-dimensional isolation systems (horizontal isolation) enables a considerable reduction in structural responses during seismic events, the size of the structural elements can be reduced resulting in a lighter structures and overall cost reduction. However the vertical responses of the horizontal base isolated buildings tend to be greater than in the non-isolated conventional buildings due to its amplification in the isolation layer and the superstructure. Therefore the reinforcement of vertical seismic supports is required depending on the type of structure and the seismic conditions. Previous research has presented multiple solutions for the mitigation of vertical structural responses associated with seismic activity.

Kato,A.,et al.[1] and Kato,M.,et al.[2] have presented a large Scale R&D Project on three-dimensional seismic isolation for Fast Breeder Reactors (FBR) in Japan, where a series of concepts for different 3D seismic isolation devices where presented and researched for feasibility. Fig.1 to Fig.4 show these concepts, where the common working principle was to use an elastomeric seismic isolator for horizontal isolation accompanied with a variety of solutions for vertical isolation. Fig.1 shows the concept of a hydraulic 3D base isolation system [3], where in the event of seismic excitation, the fluctuating vertical seismic force is converted by the load-carrying cylinders into pressure fluctuations of hydraulic fluid, each cylinder being connected through piping to an accumulator unit .The vertical restoring force to be applied to the structure is generated by the bulk modulus of the nitrogen gas confined within this accumulator unit.

Fig.2 shows a 3D isolator with metallic bellows [4], where the vertical isolation is realized by the effect of a double reinforced metallic below filled with gas. Fig.3 shows a concept using roller type air springs [5] that are permanently connected to a gas supply unit, in order to control the pressure. Additional energy dissipation is achieved by viscous fluid dampers installed in a vertical orientation. Fig.4 shows a special type of cable reinforced air spring [6] that could work simultaneously for both horizontal and vertical seismic isolation

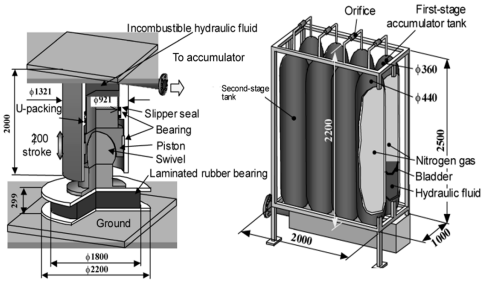

Fig. 1 – Hydraulic 3D base isolation system

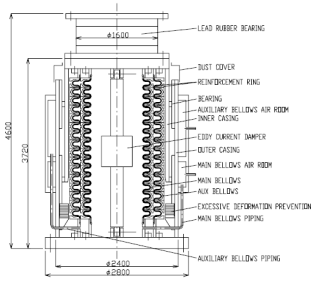

Fig. 2 – 3D isolator using metallic bellows

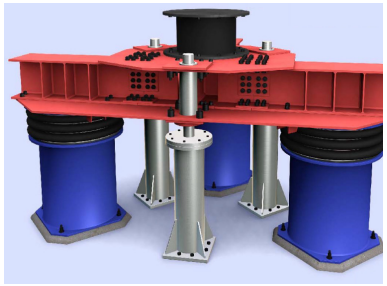

Fig. 3 – 3D seismic isolation device with rolling seal type air spring

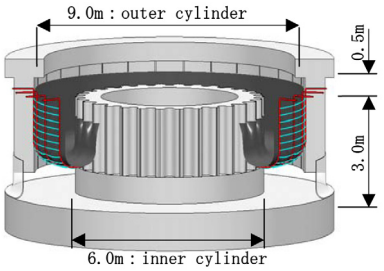

Fig. 4 – Cable reinforced 3D air spring concept

An application for 3D seismic isolation was presented by Osamu T.,et al. [7] for the construction of a residential building using the 3D seismic isolation device with a rolling seal type air spring shown in Fig.3. This application concluded that a 3D seismic isolation device should be easy to maintain, not necessary to periodically replaced, not significantly influenced by temperature, relatively easy to model in structural analysis, effective against the

vibration from very small amplitude to large amplitude and can be controlled against the structural rocking motion accompanied by vertical responses.

2. 3D rotational seismic isolator

The basic concept of the 3D rotational seismic isolator (3DRSI) is realized by combining vector algebra with the mechanical characteristics of elastomeric bearings, where it may be any type of rubber based isolators. In this research, lead rubber bearings (LRB) [8] are used. As Shown in Fig.5, When a Vertical Force F acts on an inclined Plane with inclination angle α, it is divided into components, $F.Sin\alpha$ and $F.Sin\beta$ where $\beta=90-\alpha$. This basic concept is further applied using a special configuration in order to use the horizontal behavior of lead rubber bearings to achieve the overall desired 3DRSI vertical behavior. This behavior is further explored within this study.

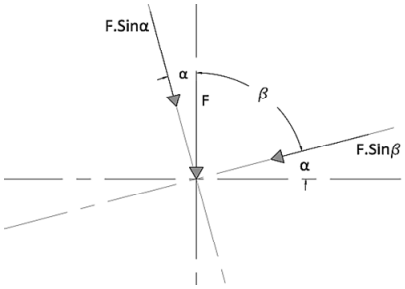

Fig. 5 – Basic concept of force resolution

As shown in Fig.6 and Fig.7, The 3DRSI is mainly composed of two parts; an upper section which consists of a LRB for horizontal isolation and a lower section which consists of a LRB group, each inclined on its X and Y axis to convert local horizontal deformation into an overall vertical deformation. Furthermore, a bearing is placed between the upper and lower sections in order to relief the upper bearing from the expected rotational motion of the lower section resulting from an applied vertical load, this rotational motion is a direct result from the inclined configuration of the lower group.

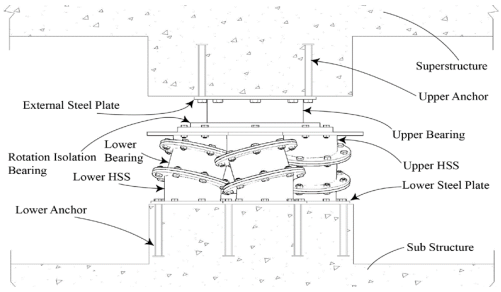

Fig. 6 – 3DRSI configuration

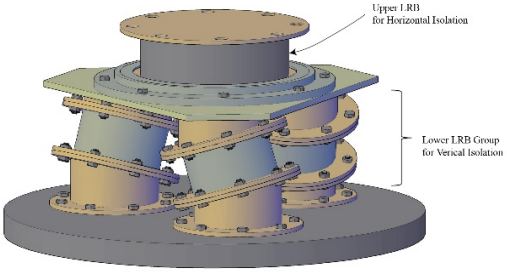

Fig. 7 – General Scheme

In the upper part, the LRB is designed according to the horizontal isolation requirements. Where it can carry a part of the horizontal load and the rest is transmitted to the lower group, however this type of load distribution can be ignored in case of using auxiliary components that have the ability to restrict the lower part in horizontal motion while allowing vertical movement. The lower steel plate attached to the LRB is free to rotate around its Z-axis by means of a recessed steel bearing, where it is designed to restrain the horizontal movement of the embedded LRB as well as providing flexibility for the expected rotational motion of the lower part. The term Rotation Isolation Bearing is used to describe this part. Fig.8 shows the elevation of the 3DRSI.

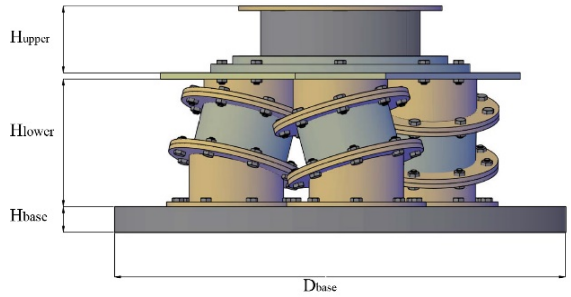

Fig. 8 – Elevation view of the 3DRSI

The lower part is composed of multiple short columns (inclination plate group) shown in Fig.9, they are typically made of hollow steel sections HSS welded to upper and lower connection steel plates, where the lower steel plate is connected to the substructure and the upper steel plate is connected to the lower group. These short columns can increase in number according to the geometric and mechanical requirements. The steel sections are designed in order to provide an inclined configuration for the lower bearings, where this inclined configuration will achieves the required inclination angle for each LRB in the lower group. The inclination angle is calculated according to the vertical design criteria and the seismic weight of the structure. Each lower LRB is inclined on its local *X* and *Y* axis as shown in Fig.10.

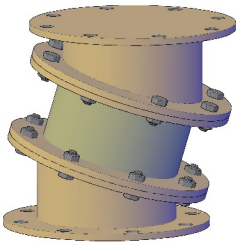

Fig. 9 – HSS-LRB assembly

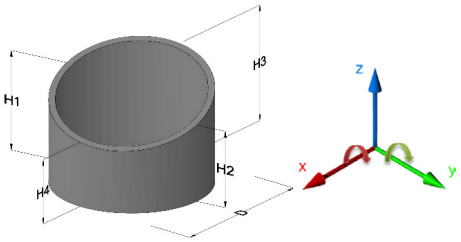

Fig. 10 – Inclination concept of lower HSS

3. Configuration and mechanical characteristics

3.1 3DRSI Geometry

The diameter of the configuration construction circle shown in Fig.11, joins the bearings of the lower group and is determined in relation with the number of bearings in the lower part as well as their maximum allowable rotation capacity.

The planar rotational motion of one bearing piece from the lower group can be determined from Eq. (1), while the overall rotation of the 3DRSI can be determined from Eq. (2):

$$\vartheta_{\text{bearing rotation}} = \sin\theta \cdot \left[180 - 2 \cdot \cos^{-1} \frac{X}{arm} \right] \quad (1)$$

$$\vartheta_{\text{3DRSI rotation}} = 180 - 2 \cdot \cos^{-1} \frac{X}{arm} \quad (2)$$

Where for one lower LRB,

$\vartheta_{\text{bearing rotation}}$: Planar rotation;

ϑ : Angle of inclination;

X : Horizontal displacement;

arm : is the radius of the imaginary circle joining the centers of the lower LRB group.

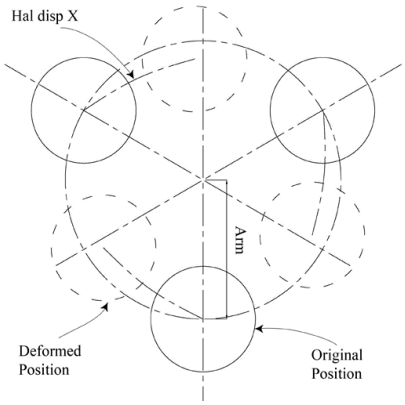

Fig. 9 – Scheme of lower LRB deformation

3.2 Mechanical characteristics

Based on the illustrated 3DRSI components, it can be modeled using spring-damper link elements as shown in Fig.12, where the upper part is based on the properties of the upper LRB, while the lower part is based on the combined properties of the lower group along with the inclination effect.

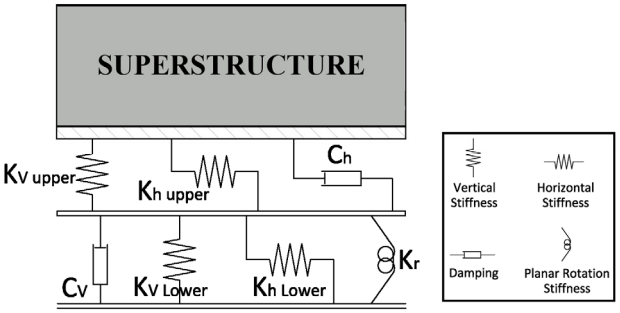

Fig. 12 – 3DRSI stiffness model

The design parameters of an individual LRB are not discussed, however the authors chose to explain the design parameters of the fully assembled 3DRSI taking into account the effects of the upper and lower parts as well as explaining the significant parameters of the lower part assembly.

Each one of the LRBs in the LRB group is inclined by angle ω_x and ω_y on its local X and Y axis respectively, as a result, the corresponding properties in the vertical and horizontal directions will vary with the degree of inclination. The following calculations are based on an inclination angle θ equivalent to ω_y. The horizontal post yield stiffness K_d, the effective stiffness K_{eff}, characteristic strength Q_d and vertical stiffness K_v of a single LRB from the lower group can be obtained by the same method used for the upper LRB.

3.3 Compression characteristics of the lower group

The compressive post yield stiffness $K_{v.Lower}$ is expressed in terms of the local characteristics of the inclined lead rubber bearings as shown in Eq. (3),

$$K_{v.Lower} = \left[\frac{N \cdot \left(\frac{K_v}{Cos^2\theta} \right) \cdot \left(\frac{K_d}{Sin^2\theta} \right)}{\left(\frac{K_v}{Cos^2\theta} \right) + \left(\frac{K_d}{Sin^2\theta} \right)} \right]_{Lower}$$

$$K_{v.Lower} = \left[\frac{N \cdot K_v \cdot K_d}{\left(K_v \cdot Sin^2\theta \right) + \left(K_d \cdot Cos^2\theta \right)} \right]_{Lower} \quad (3)$$

where N is the number of bearings used.

The compressive yield load $Q_{v.Lower}$ is dependent on the characteristic strength of the inclined LRB and is expressed in Eq. (4),

$$Q_{v.Lower} = \left[\frac{N \cdot Q_d}{Sin\theta} \right]_{Lower} \quad (4)$$

while Eq. (5) expresses the compressive effective stiffness $K_{v.eff.Lower}$.

$$K_{v.eff.Lower} = \left[\frac{N \cdot K_v \cdot K_{eff}}{\left(K_v \cdot Sin^2\theta \right) + \left(K_{eff} \cdot Cos^2\theta \right)} \right]_{Lower} \quad (5)$$

The maximum vertical load that can be applied to the lower LRB group is bounded by the buckling limit and the rotation stability of each LRB at a given shear strain value. Where the critical buckling stress σ_{cr} at a load P_{cr} is typically given by Eq. (6) [9],

$$\sigma_{cr} = \zeta G S_1 S_2 \quad (6)$$

Where, $\zeta = \pi \sqrt{\frac{\kappa}{8\left(1 + 2\kappa S_1^2 G / E_b\right)}}$

The first and second shape factors S_1 and S_2 for circular and rectangular cross-sections are determined from Eq. (7) and Eq. (8) respectively [10].

$$S_{1.Circular} = \frac{d_0}{4t_r}$$

$$S_{1.\text{Rectangualr}} = \frac{a \times b}{2(a+b)t_r} \quad (7)$$

$$S_{2.Cricular} = \frac{d_0}{T_r}$$

$$S_{2.\text{Rectangular}} = \frac{a}{T_r} \quad (8)$$

The maximum vertical load $P_{\max}$ is expressed as the least of the two expressions given in Eq. (9),

$$P_{\max} = \left[N \cdot P_{cr} \cdot Sec\theta \cdot \left(1 - \frac{\gamma}{0.9 S_2} \right) \right]_{Lower}$$

$$P_{\max} = \left[N \cdot Csc\theta \cdot \left(Q_d + \gamma \cdot T_R \cdot K_d \right) \right]_{Lower} \quad (9)$$

where, the typical maximum value of shear strain $\gamma_{\max}$ of one LRB shall not exceed 200% [11], however based on the observation of experimental results, the authors would recommend a maximum of 150% shear strain in design conditions γ_{design} .

The maximum vertical displacement $Z_{\max}$ can then be obtained from Eq. (10),

$$Z_{\max} = \frac{P_{\max}}{K_{v.eff.Lower}} \tag{10}$$

While the equivalent horizontal viscous damping ratio can be derived from Eq. (11),

$$\beta_v = \frac{1}{2\pi}\left(\frac{EDC_v}{P_d \cdot Z_d}\right) \tag{11}$$

where, EDC_v: the energy dissipated per cycle under compression loads ; V_d: design vertical compression load.

3.4 Horizontal characteristics of the lower group

The horizontal post yield stiffness can be determined by Eq. (12).

$$K_{d.Lower} = \left[\frac{N \cdot K_v \cdot K_d}{\left(K_v \cdot Cos^2\theta\right) + \left(K_d \cdot Sin^2\theta\right)}\right]_{Lower} \tag{12}$$

Similar to the compressive yield load, the horizontal yield load is dependent upon the characteristic strength of the inclined LRB and is can be expressed by Eq. (13).

$$Q_{d.Lower} = \left[N \cdot Q_d \cdot Sec\theta\right]_{Lower} \tag{13}$$

The horizontal effective stiffness $K_{eff.Lower}$ is expressed by Eq. (14).

$$K_{eff.Lower} = \left[\frac{N \cdot K_v \cdot K_{eff}}{\left(K_v \cdot Cos^2\theta\right) + \left(K_{eff} \cdot Sin^2\theta\right)}\right]_{Lower} \tag{14}$$

3.5 Global characteristics of the 3DRSI

The global characteristics of the 3DRSI are a combination of the upper and lower LRB properties. The effective compressive stiffness $K_{v.eff.3DRSI}$ and the compressive yield load of the 3D RSI are expressed by Eq. (15),

$$K_{v.eff.3DRSI} = \frac{K_{v.upper} \cdot K_{v.eff.Lower}}{K_{v.upper} + K_{v.eff.Lower}} \tag{15}$$

while the compressive yield load $Q_{v.3DRSI}$ is equivalent to that of the lower LRB group and can be obtained from Eq. (4). The horizontal post yield stiffness $K_{d.3DRSI}$ and the yield load $Q_{d.3DRSI}$ of the 3D RSI are expressed in Eq. (16) and Eq. (17) respectively.

$$K_{d.3DRSI} = \frac{K_{d.upper} \cdot K_{d.Lower}}{K_{d.upper} + K_{d.Lower}} \quad (16)$$

$$Q_{d.3DRSI} = \frac{Q_{d.upper} \cdot Q_{v.Lower}}{Q_{d.upper} + Q_{v.Lower}} \quad (17)$$

The terms relating to the lower group in Eq. (16) and Eq. (17) can be ignored in case of using any type of auxiliary horizontal guides, where Fig.13 shows an example guiding configuration. In such a case, the 3DRSI can be considered to be rigid in the horizontal direction at the lower group, where the horizontal characteristics of the 3DRSI will then only be dependent on the properties of the upper LRB.

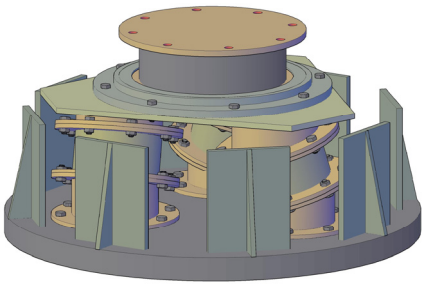

Fig. 13 – 3DRSI with horizontal guides

4. Prototype testing

4.1 Test Machine

The 3DRSI was tested for feasibility, concept confirmation and mechanical properties. A compression test machine was used to experiment the vertical properties, while the horizontal properties were not tested assuming that an auxiliary device is used in order to achieve horizontal rigidity. The compression test machine is shown in Fig.14. The vertical load is applied by a 2000 kN oil jack that has a maximum vertical displacement capacity of 500 mm, where the maximum loading speed is 60 mm/min.

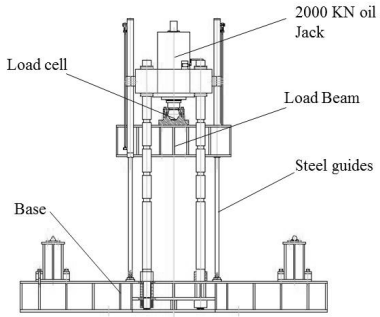

Fig. 14 – Scheme of test machine

4.2 Prototypes

The manufactured prototype of the 3D RSI is shown in Fig.15 where the key component was the lower HSS. Fig.16 shows a typical cross-section of the lead rubber bearing used. Three types of HSS were fabricated in order to achieve 10^0 and 20^0 angles of inclination respectively. Finally an upper hexagonal steel plate was placed above the assembled short columns acting as the load distributor.

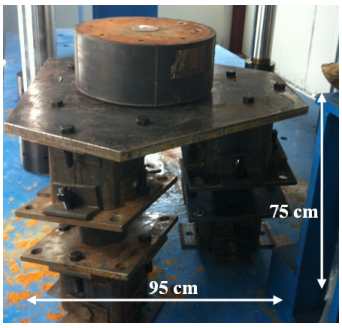

Fig. 15 – 3DRSI prototype

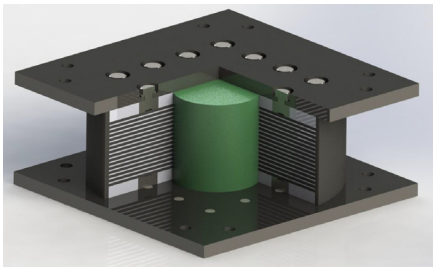

Fig. 16 – Lead rubber bearing

4.3 Test Specimens and procedures

Three types of LRB specimens were used in this testing procedure, where the geometrical properties of each specimen are shown in Table 1, while, Table 2 shows the material properties of the elastomers used, where it is noted that LRB100-2 and LRB100-3 test specimens share the same material properties while LRB100-1 is different. It also noted that the test specimens were design in a way to have variable first and second shape factors S_1 and S_2 respectively, The reason for that was to confirm the previously derived theoretical assumptions for the characteristics and study their dependencies, as it was found that the vertical properties of the 3DRSI vary with the change of S_1 and S_2.

Table 1: Characteristics of test specimens

Parameter		**LRB100-1**	**LRB100-2**	**LRB100-3**
Diameter [mm]		100	100	100
Lead core diameter [mm]		14	20	20
Inner rubber layers	Thickness [mm]	1.3	2	1.0
	Number [-]	11	15	13
Inner steel plates [mm]		2	2	2
Total rubber thickness [mm]		14.3	30	13
1st Shape factor S_1 [-]		19.23	12.5	25
2nd Shape factor S_2 [-]		6.99	3.33	7.69
Critical stress [MPa]		64.4	35.3	139.45

Table 2: Elastomer properties for test specimens

Ref. type	**G [N/mm²]**	**E_b [N/mm²]**	**E_0 [N/mm²]**	**κ[-]**	**σ_{Pb} [N/mm²]**
LRB100-1	0.55	1960	1.65	0.78	10.5
LRB100-2	0.9	1960	2.7	0.6	10.5
LRB100-3					

The loading scheme shown in Table 3 was chosen to confirm the 3DRSI vertical load capacity and to obtain the effective vertical stiffness, Tests were performed for 4 cycles using 10^0 and 20^0 angles of inclination.

Table 3: Loading procedure for test specimens

Test	P_{min} [kN]	P_{max} [kN]	Test	P_{min} [kN]	P_{max} [kN]
LRB-1 with 10^0 inclination			LRB-2 with 20^0 inclination		
LRB-1-I10-Step1	20	80	LRB-2- I20-Step2	20	80
LRB-1- I10-Step2	40	120			
LRB-1- I10-Step3	20	120			
LRB-1- I10-Step4	40	200			
LRB-1 with 20^0 inclination			LRB-3 with 10^0 inclination		
LRB-1- I20-Step1	20	80	LRB-3- I10-Step1	20	80
LRB-1- I20-Step2	40	100	LRB-3- I10-Step2	50	80

4.4 Test Results and discussion

Fig.17 to Fig.25 show the output vertical load - vertical displacement plots for the performed steps in Table 3. A comparison between the design effective vertical stiffness and that obtained by testing is shown in Fig.30. It can be seen that the cyclic behavior, energy dissipation and returning force for LRB1 and LRB2 are better that of LRB2, where this is mainly due to the low S_1 and S_2 of LRB2, even though it has a bigger lead core. Additionally, it can be seen that under the same loading conditions LRB1 achieved a higher vertical displacement than LRB3, whereas LRB1 has a lower shape factor compared to LRB3.

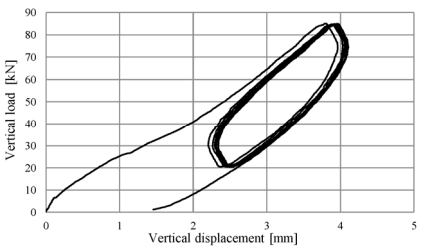

Fig. 17 – LRB-1-I10-Step1

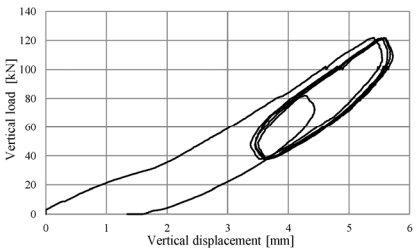

Fig. 18 – LRB-1- I10-Step2

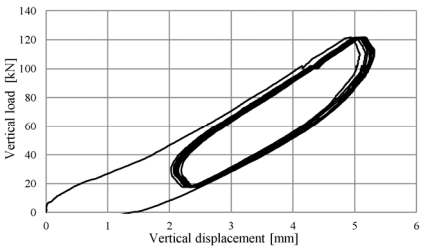

Fig. 19 – LRB-1- I10-Step3

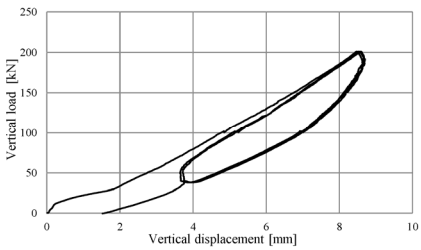

Fig. 20 – LRB-1- I10-Step4

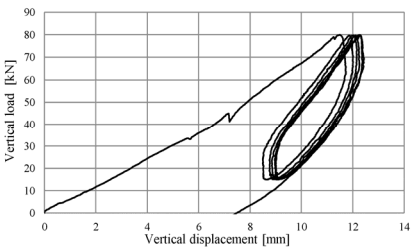

Fig. 21 – LRB-1- I20-Step1

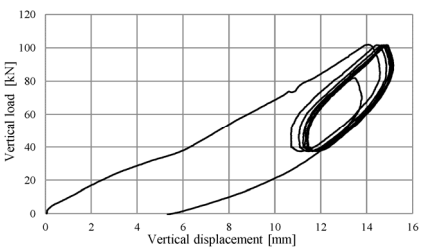

Fig. 22 – LRB-1- I20-Step2

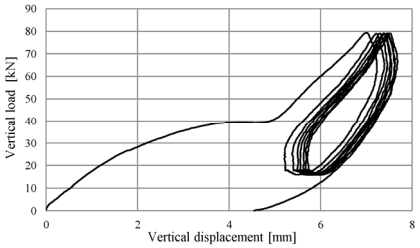

Fig. 23 – LRB-2- I20-Step2

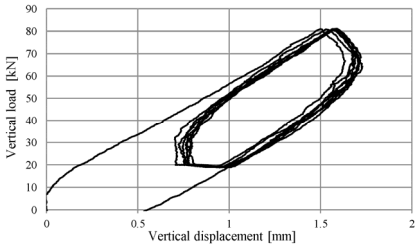

Fig. 24 – LRB-3- I10-Step1

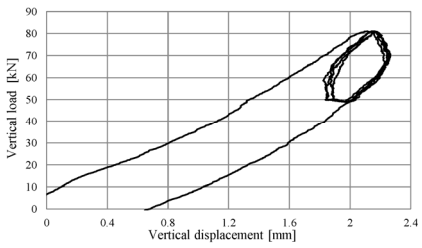

Fig. 25 – LRB-3- I10-Step2

Further study, by numerical analysis, of the relationship between the 3DRSI characteristics and the lower LRB shape factors showed that for the same lower LRB diameter, the variation in S_1 at a constant S_2 with different inclination angles, shown in Fig.26a and Fig.26b, does not result in a significant change in the vertical or horizontal stiffness's of the 3DRSI. On the other hand, shape factor variances had a bigger effect on the overall maximum vertical load and displacement capacities. Figures 27a to 27d show the effect of variation in S_1 at a constant S_2 on the 3DRSI vertical load capacity at different inclination angles, where all calculations were based on LRB with a 300 mm effective diameter and a 60 mm lead core, where $N=3$.

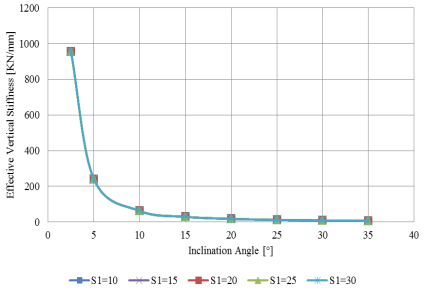

(a) At S_2=3

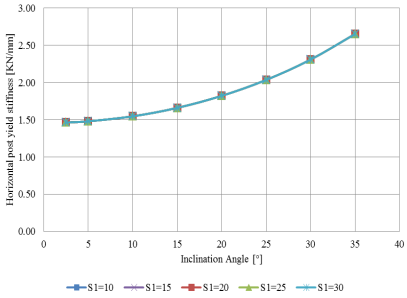

(b) At S_2=3

Fig. 26 – Effect of S_1 on [*Kv* and *Kd*-inclination angle] at a constant S_2

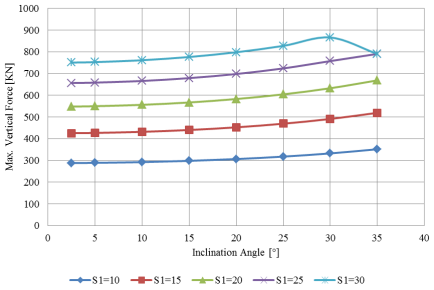

(a) At S_2=3

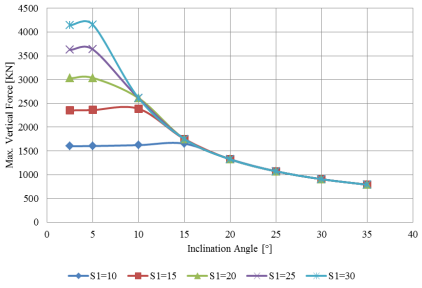

(b) At S_2=4

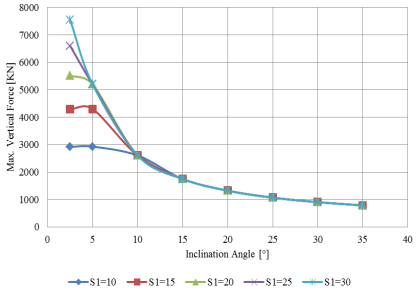

(c) At S_2=5

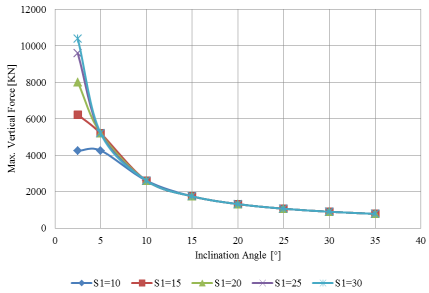

(d) At S_2=6

Fig. 27 – Effect of S_1 on the [P_{max}-inclination angle] at a constant S_2

From Fig.28, for LRB1 and LRB3, the difference between the effective vertical stiffness obtained from design and testing was within a 10% range. For LRB2, it can be seen that the difference is within 35%. The inconsistency of the test results for LRB2 was further concluded to be directly related to the low shape factors of this specimen. Furthermore, the high ratio between the effective diameter of rubber and the lead core diameter resulted in a poor overall vertical returning moment for the 3DRSI.

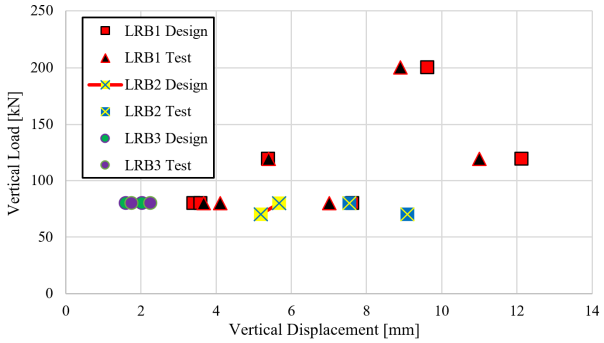

Fig. 28 – Effective vertical stiffness (experimental-design values)

A comparison between the theoretical and experimental values at the 3rd loading cycle for the EDC is shown in Table 4.

Table 4: comparison between design and experimental output for the energy dissipated per cycle

Test	EDC (test) [kN·mm]	EDC (design) [kN·mm]	Error [%]	β_v [%]
LRB100-1-I10 Step1	43.07	40.35	6.74	5.95
LRB100-1-I10 Step2	70.12	64.17	9.26	5.11
LRB100-1-I10 Step3	108.10	100.72	7.32	4.45
LRB100-1-I10 Step4	224.19	203.94	9.93	4.06
LRB100-1-I20 Step1	77.86	72.6	7.24	5.5
LRB100-1-I20 Step2	103.01	94.28	9.26	5.95
LRB100-2-I20 Step2	45.37	49.08	-7.56	6.51
LRB100-3-I10 Step1	23.71	21.95	8.02	5.82
LRB100-3-I10 Step2	6.41	5.99	7.04	6.36

Fig.29 and Fig.30 show snapshots from the LRB1 specimen testing, where Fig.24 shows the horizontal deformation behavior as a result of the applied vertical load, while Fig.25 shows the relative motion between the upper and lower plates of the LRB1 specimen, where is clear that each lower LRB experiences deformation along its *X* and *Y* axis, as well as planar rotation along its local axis. This relative movement confirms the basic principle of the 3DRSI.

Fig. 29 – 3DRSI vertical deformation

Fig. 30 – Relative movement of upper and lower steel plates

4.5 Summary of prototype testing

The 3DRSI was tested for feasibility, concept confirmation and mechanical properties. A compression test machine was used in investigating the vertical properties of the 3DRSI. Through-out the testing of three LRB specimens in the lower group, the concept of 3DRSI was confirmed. The overall vertical deformation corresponded to the lower LRB horizontal deformation along with the rotational motion for the upper hexagonal plate. It is also worth mentioning that each LRB experienced planar rotation about its local axis. The effective vertical stiffness obtained by testing was compared to that obtained by design, where the theoretical calculations were very similar to the test output, which confirms the previously defined design procedure. Finally the energy dissipation characteristics obtained, correlated with the design data with a margin of ±10%.

5. Conclusion

The target of this research was achieved by the development of the concept, definition of components, developing the design procedure and testing of a new 3D seismic isolator. Prototype testing has confirmed the principle of the 3DRSI showing that the results were in great proximity of the design parameters, however testing also showed the variation of the vertical characteristics depending on the degree of inclination of the lower group, shape factors, and lead core size.

It is worth mentioning that testing also showed the complex deformation introduced to the Lead Rubber bearings, where in addition to the planar deformation of the lower group, there was a rotational motion about the local Z-axis of each LRB. This rotational motion was rather hard to define numerically in relation to the LRB mechanical properties. Testing showed that rotation stiffness was very small and could be neglected; however the effect of cyclic rotation could result in the deterioration of the LRB horizontal performance. This part should be the subject of future investigations.

While the permanent horizontal shear strain applied on the each of the lower group Lead Rubber Bearings is a key parameter in the function of the 3DRSI, it also introduces a permanent loading case on the LRBs which was not properly researched before. The authors see that such a loading case may be avoided by using mechanical or hydraulic fuses in the vertical direction.

6. Acknowledgement

This research was funded by the National Natural Science Foundation of China, grant number 51278291, 51478257, 51308331, Ph.D. Programs Foundation of Ministry of Education of China (20133108110024), and Natural Science Foundation of Shanghai (15ZR1416200).

7. References

[1] Kato,A.,et al. A large Scale Ongoing R&D Project on Three-Dimensional Seismic Isolation for FBR in Japan, 2002ASME PVP, Seismic Engineering.

[2] Kato,M.,et al. Design study of the seismic-isolated reactor building of demonstration FBR plant in Japan. 13th SMiRT, Aug.1995, pp579-584.

[3] Akihiro K., Takahiro S., Tatsuya F., Satoshi M.. Study on 3-Dimensional Base Isolation System Applying to New Type Power Plant Reactor (Hydraulic 3-Dimensional Base Isolation System: No.1). Transactions of the 17th International Conference on Structural Mechanics in Reactor Technology (SMiRT 17) Prague, Czech Republic, August 17 –22, 2003.

[4] Seitaro O., Kyotada N., Michiaki S., Satoshi M.. Development of 3D Seismic Isolator using Metallic Bellows. Transactions of the 17th International Conference on Structural Mechanics in Reactor Technology (SMiRT 17) Prague, Czech Republic, August 17 –22, 2003.

[5] Junji S., Tadashi T., Kazuya O., Yasuo O., Satoshi M.. Research on 3-D Base Isolation System Applied to New Power Reactor 3-D Seismic Isolation Device with Rolling Seal Type Air Spring : Part 1. Transactions of the 17th International Conference on Structural Mechanics in Reactor Technology (SMiRT 17) Prague, Czech Republic, August 17 –22, 2003.

[6] Mitsuru K, Tsutomu, I b, Katsuhiko U, Takahiro S, Satoshi M. Development of Three - Dimensional Base Isolation System with Cable Reinforcing Air Spring. Transactions of the 17th International Conference on Structural Mechanics in Reactor Technology (SMiRT 17) Prague, Czech Republic, August 17 –22, 2003.

[7] Osamu T., Hiromasa A.,Junji S., Ryoichiro M.,Yasuo T.,Takafumi F.. Construction of Civil Building Using Three Dimensional Seismic Isolation System (Part 1, Design of Building Using Three Dimensional Seismic Isolation System). The 14th World Conference on Earthquake Engineering October 12-17, 2008, Beijing, China.

[8] Kelly J. M. Earthquake Resistant Design with Rubber[M]. Second Edition. 1997. Springer Verlag London Limited.

[9] Liu WG. Analysis of seismic response of the mechanical properties of rubber isolators and isolated structures[D]. Beijing University of Technology PhD thesis, 2003.

[10] International Standard ISO 22762:2010 for Elastomeric seismic-protection isolators. International Organization for Standardization, November 2010.

[11] Symans M. D., Seismic Protective Systems: Seismic Isolation. Instructional Material Complementing FEMA 451, Design Examples, 2004.